PAPER

Check for updates

Three-dimensional Ni$_4$O$_4$-cubane metal–organic framework as a high-performance electrocatalyst for urea oxidation†

Mariam Batool, [a] Amir Waseem [a] and Muhammad Arif Nadeem [*ab]

The urea oxidation reaction (UOR) is considered to be a replacement of the sluggish anodic oxygen evolution reaction (OER) in overall water-splitting. A three-dimensional (3D) nickel-containing metal–organic framework $\{[Ni^{II}_2(pdaa)(OH)_2(H_2O)]\}_n$ (**MOF 1**) (where, H$_2$pdaa = 1,4-phenylene diacetic acid) was investigated as a robust and highly efficient electrocatalyst for the UOR. **MOF 1** comprised 1D nickel(II) chains crosslinked through Ni$_4$O$_4$ cubane units to form a 3D extended network. Dangling Ni···OH$^-$ groups were exposed in the **MOF 1** structure, and could act as active catalytic centers for the UOR. **MOF 1** required a very small onset potential of 1.18 V for urea oxidation in KOH (1 M) and urea (0.33 M) and had a low Tafel slope of 38.8 mV dec^{-1} (in contrast to 1.84 V for the oxygen evolution reaction). The overpotential required to attain a catalytic current density of 10 mA cm^{-2} was 1.24 V, which is much lower than that for many materials. Controlled potential electrolysis, powder X-ray diffraction, and X-ray photoelectron spectroscopy affirmed the physicochemical integrity of the catalyst over a 17 h test reaction. This work not only addresses the problem of urea contamination, it also helps to utilize it in an energy-conversion process.

Introduction

Efficient energy carriers with high energy density, low cost, and ease of availability are needed worldwide.[1] Hydrogen is considered to be a promising candidate for replacement of fossil fuels because it has high energy density and is environmentally friendly (the only by-product is H$_2$O).[2,3] Electrolyzing water is an old (yet promising) route for hydrogen production because of its high purity. Electrocatalytic water-splitting involves a cathodic hydrogen evolution reaction (HER) and anodic oxygen evolution reaction (OER). However, due to the high kinetic barriers (1.23 V) associated with multiple electron-coupled proton processes in OER, following this route is difficult.[4] The actual working potential usually increases to 1.8 V due to the torpid kinetics of OER and HER, resistance from the electrolyte and electrode material, and their contact resistance.[5,6] To minimize these factors, several solutions have been suggested, such as using suitable electrocatalysts to amplify

slow kinetics, modifying electrolyzer structure, and substituting the OER with other promising anode reactions.[7–9]

Substitution of the OER by readily oxidized chemicals have gained the attention of the scientific community, and use of hydrazine, alcohols, amines, aldehydes and urea has been suggested.[10–14] Among these, the urea oxidation reaction (UOR) is preferred due to low thermodynamic voltage (0.37 V *vs.* reversible hydrogen electrode (RHE)), non-toxicity, stability, abundance, as well as ease of transportation and storage.[15,16] In addition to industrial (*N*-containing fertilizers) and agricultural production, urea is produced as a bio-waste that pollutes the atmosphere and groundwater. It has been estimated that 80% of wastewater is dumped each year.[17] The natural decomposition of urea releases nitrates and ammonia, which cause eutrophication and severe hazards to the environment and health.[18] Therefore, the UOR is not only a good way to produce hydrogen efficiently, it can also be a remedy for wastewater treatment.[19,20] The UOR (like the OER) is a complex process that involves transfer of six electrons with a complex system of gas evolution.[13]

The oxidation of urea over noble metals (*e.g.*, Ti–Pt, Ti–Pt–Ir and Ru–TiO$_2$) has been studied by several research teams. However, high cost and poisoning of the surface catalyst limits practical application.[21–24] Boggs and colleagues documented the electro-oxidation of urea by cost-effective Ni-based catalysts in a basic medium.[25] The facile oxidation of Ni(II) to Ni(III) during electrocatalysis makes it a promising candidate for the UOR.[26] Moreover, the consistency between the peak of urea oxidation

aCatalysis and Nanomaterials Lab 27, Department of Chemistry, Quaid-i-Azam University, Islamabad 45320, Pakistan

bPakistan Academy of Sciences, 3-Constitution Avenue Sector G-5/2, Islamabad, Pakistan. E-mail: manadeem@qau.edu.pk; Tel: +92-51-9064-2062

† Electronic supplementary information (ESI) available: SEM image, FT-IR spectrum, TGA, coordination environment for Ni, cyclic voltammograms for C_{dl}, LSV at varied scan rates, post-catalytic SEM and XPS survey of **MOF 1**. See https://doi.org/10.1039/d2ra05145a

and peak of Ni oxidation makes Ni-based catalysts active for urea oxidation.[27,28] This approach led the scientific community in the last decade to search for Ni-based catalysts to understand the reaction mechanisms.[29,30] Ni-containing electrocatalysts have been employed for the UOR. For instance, Ni_3N nanosheet arrays have been reported to be active catalysts for the UOR, with a small onset potential of 1.33 V vs. RHE.[31] Similarly, an onset potential of 1.35 V has been documented for $Ni_{0.9}Fe_{0.1}O$ porous hollow microspheres.[32] Also, an onset potential of 1.36 V for $Ni(OH)_2$ leads to an effective UOR.[15] Zhang and colleagues demonstrated UOR activity for Ni–Mo nanotubes at 1.36 V vs. RHE.[33]

Metal–organic frameworks (MOFs) have many metal cations on their surface, electronic structures to attain high oxidation states, unsaturated metal sites, and are versatile. These features make MOFs promising electrocatalysts for the UOR.[34] Their three-dimensional (3D) structure provides high specific surface area and facilitates mass transport to enhance electrocatalytic activity.[35–39] Recently, $NiFe-MIL-53-NH_2$ was shown to elicit a better UOR with an onset potential of 1.36 V compared with its monometallic counterparts $Fe-MIL-53-NH_2$ (1.61 V) and $Ni-MIL-53-NH_2$ (1.42 V).[40] The Ni-MOF@NiO/Ni composite demonstrated electrocatalytic urea oxidation at 1.40 V for 10 mA cm^{-2}.[41] Pang and colleagues reported 3D aggregates of Ni-MOF ultrathin nanosheets to display a potential of 1.38 V for the UOR at 10 mA cm^{-2},[42] and ultrathin 2D Ni-MOF has been reported to produce identical current density at a potential of 1.36 V.[43] Due to the instability of certain MOFs under electrochemical conditions, MOF-derived Ni/C electrocatalysts have been reported to display the onset of urea oxidation at 1.33 V.[44] Rezaee and co-workers discovered that $Ni_{1.6}Co_{0.4}P/C@HCNs$ fabricated from NiCo-MOF could produce 10 mA cm^{-2} at a potential of 1.33 V.[45] Optimizing UOR catalysts via compositional modulation and microstructure design could enhance UOR performance.

We report a 3D MOF, $\{[Ni^{II}_2(pdaa)(OH)_2(H_2O)]\}_n$ (MOF 1), as a highly efficient electrocatalyst for urea oxidation synthesized via a hydrothermal approach. The exceptionally low onset potential of 1.18 V vs. RHE in contrast to the sluggish OER (onset potential of 1.84 V) and small Tafel slope (38.8 mV dec^{-1}) was displayed by MOF 1. For the UOR, a 3D MOF having such a low overpotential of 1.24 mV to achieve a catalytic current density of 10 mA cm^{-2} has not been documented. The controlled potential electrolysis (CPE) for 17 h continuously depicts the stability and robustness of MOF 1. We describe a cost-effective electrocatalyst for water-splitting but also propose a hybrid water electrolysis-affiliated urea oxidation to substitute the torpid OER for H_2 generation. This strategy would aid energy conversion and treatment of wastewater by electrochemical means.

Experimental

Synthesis of MOF 1

The synthesis of MOF 1 was carried out according to our method, which has been reported previously.[46] Briefly, a mixture of 1,4-phenylene diacetic acid (pdaa; 0.5 mmol) and KOH (2 mmol) was stirred for 10 min in distilled water (6 mL). $NiCl_2\cdot6H_2O$ (1 mmol) was dispersed in water (4 mL) and added slowly to the reaction mixture. This mixture was transferred to a 23 mL autoclave and kept at 170 °C under autogenous pressure for 72 h. Green, diamond-shaped crystals were obtained after cooling to room temperature and used for characterization and electrochemical studies.

Preparation of MOF 1-deposited fluorine-dopped tin oxide electrode (FTO)

FTO of area (1×2 cm^2) was washed successively with deionized water and alcohol by sonication. Then, it was kept in a furnace at 400 °C for 30 min for annealing, and used for catalytic studies. The catalytic suspension was prepared by pouring 5 μL of Nafion (binder) over MOF 1 (2 mg) and ethanol (1 mL). This mixture was sonicated for 1 h to obtain a homogenous ink, drop-casted over annealed FTO, and dried overnight at 50 °C in a desiccator before electrocatalytic studies.

Electrochemical measurements

Electrochemical experiments were carried out in a potentiostat (Gamry Interface 5000) electrochemical analyser. A three-electrode system (FTO-coated electrode (working), Hg/HgO (reference), and graphite rod (counter electrode)) was used at room temperature. All potentials were transformed into a reversible hydrogen electrode (RHE) using

$$E_{RHE} = E_{Hg/HgO} + 0.0592 \,(pH) + 0.098$$

Before electrochemical testing, N_2 gas was bubbled through the electrolyte for 30 min KOH (1 M) was used as the electrolyte for the OER. A mixture of KOH (1 M) with urea (0.33 M) was used to carry out studies on urea oxidation. The electrocatalytic performance was evaluated by linear sweep voltammetry (LSV). CPE was employed to check the stability of MOF 1. Cyclic voltammetry (CV) was done in a non-faradaic region to estimate double-layer capacitance (C_{dl}) in the narrow potential at sweep rates from 2 mV s^{-1} to 14 mV s^{-1}. Potentiostatic electrochemical impedance spectroscopy (EIS) was carried out to evaluate impedance. All experiments were undertaken under a N_2 atmosphere.

Results and discussion

The synthesized MOF 1 was characterized by powder X-ray diffraction (PXRD), scanning electron microscopy (SEM), infrared (IR) spectroscopy, and thermogravimetric analysis (TGA). The phase purity of MOF 1 was evaluated by PXRD. Consistency with the calculated pattern implied a successful synthesis, showing major peaks at 7.7°, 11.5°, 15.5° and 18.2° (Fig. 1d). All peak positions were in accordance with a simulated PXRD pattern from a single crystal. Moreover, the sharpness of peaks showed the crystalline nature of the material.[46] When studying electrochemical properties, the shape and morphology of a material have crucial roles. High-magnification SEM
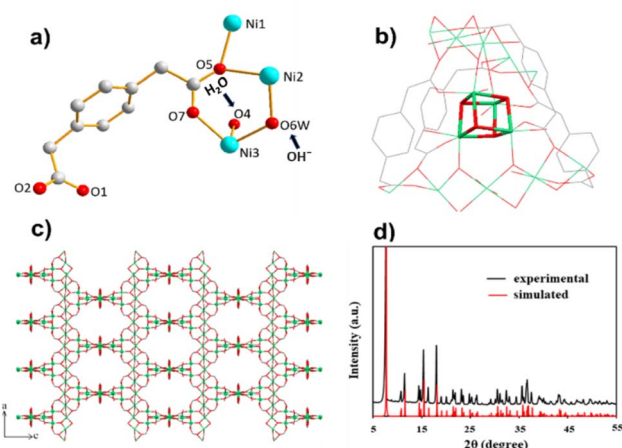
Fig. 1 (a) Asymmetric unit of **MOF 1**. (b) Fragment emphasizing interconnections between Ni chains and Ni_4O_4 cubane units. (c) Packing diagram of **MOF 1** demonstrating the separation of linear Ni chain through Ni_4O_4 cubane units. Ni: green, O: red C: grey sticks. H atoms have been omitted (d) comparison of PXRD of experimental (black) and calculated (red) patterns.

revealed a pyramidal morphology (Fig. S1†). Fourier transform (FT)-IR spectroscopy verified the synthesis of **MOF 1** because the peaks matched well with reported data (Fig. S2†). A broad peak at 3353 cm^{-1} indicated the presence of hydroxyl groups (a water molecule on the Ni ion).[41] A sharp peak at 1558 cm^{-1} appeared due to the C=O stretching. Peaks at 1260 and 1386 cm^{-1} were ascribed to the –COO– group of pdda coordinated to Ni(II).[47] Peaks below 1000 cm^{-1} were assigned to Ni–O bending and stretching vibrations.[48] The thermal stability of **MOF 1** was assessed through TGA: it showed thermal stability up to 380 °C (Fig. S3†).

Crystallographic studies revealed that 3D **MOF 1** crystallized in the tetragonal space group $I4_1/a$. The basic structural unit of **MOF 1** is shown in Fig. 1a. Structurally, **MOF 1** showed two features. The first feature was a linear Ni atom bonded octahedrally to four oxygen atoms from four pdaa ligands, and the two O atoms from two non-identical OH$^-$ gave a slightly distorted octahedral geometry. The second feature was distorted Ni cubane units bridging linear chains. The nickel center was attached to three O atoms of the bridging –OH$^-$ groups of cubane, one O atom of the pdaa ligand, one O atom of the water molecule, and one O atom that linked the nickel center to linear chains (Fig. 1b). The coordination environment of Ni sites with O atoms is shown in Fig. S4.† The 3D network was formed by the bridging of cubanes with linear Ni chains coordinated by flexible pdaa ligands (Fig. 1c). The oxidation state of +II for Ni was confirmed by bond-valence sum analysis ($\Sigma_{bv}(Ni(II) = 1.993–2.168)$).[46]

Electrocatalytic studies on urea oxidation

Several electrocatalytic methods were used *via* a three-electrode arrangement to determine the electrocatalytic performance of **MOF 1** for urea oxidation. Fig. 2a depicts the LSV of **MOF 1** fabricated on FTO in different electrolyte setups at a sweep rate

of 5 mV s^{-1}. The estimated urea concentration in human urine is 0.33 M, so this concentration was used for the UOR.[49] Fig. 2a depicts that the OER occurred in KOH (1 M) with an onset potential of 1.84 V (*vs.* RHE), which was reduced greatly to 1.18 V (*vs.* RHE) by urea addition. The current density also enhanced markedly. The as-synthesized **MOF 1** exhibited better performance for urea oxidation (1.24 V @ 10 mA cm^{-2}) than most of the recently reported Ni-based electrocatalysts given in Table 1. LSV of **MOF 1** at various scan rates is shown in Fig. S6.† The extraordinary UOR catalysis of **MOF 1** could be studied further by Tafel plots calculated from LSV curves. The lower Tafel slope of 38.8 mV dec^{-1} (Fig. 2b) compared with the OER (188 mV dec^{-1}) indicated favorable kinetics, which is a preferable feature for commercial applications. This value (in mV dec^{-1}) is lower than that reported previously: Ni(OH)$_2$ (40),[50] IrO$_2$ (70),[51] Pt/C (187),[43] aggregated Ni-MOF ultrathin nanosheets (52)[42] and Ni$_3$N NA/CC (57).[31] The excellent performance for urea oxidation can be attributed to the 3D porous structure, which facilitates electrolyte diffusion and mass transport.

The overall performance of a catalyst is dependent upon two major factors: the abundance of active sites and the intrinsic activity of each active site. We used C_{dl} to measure the electrochemical active-surface area (ECSA) to gain understanding about the intrinsic surface activity. C_{dl} was calculated by carrying out CV (Fig. 2d and S5†) in a non-faradaic region (1.065–1.165 V). The straight line acquired by plotting current density *vs.* scan rate (2–14 mV s^{-1}) at a constant potential of 1.11 V gave C_{dl}. Fig. 2e shows C_{dl} (mF cm^{-2}) of **MOF 1**, Ni(OH)$_2$, Pt/C, and bare FTO to be 47, 13, 11, and 0.9, respectively. A C_{dl} of 47 mF cm^{-2} indicates a high ECSA, thereby revealing a high density of active sites of **MOF 1** responsible for phenomenal UOR activity. Thus, the enhanced electrochemical activity could be credited to the intrinsic high activity of **MOF 1**. The corresponding ECSA was calculated as ECSA = C_{dl}/C_s (where specific capacitance (C_s) = 60 µF cm^{-2}).[40] The highest value of ECSA (in cm^2) was 783 for **MOF 1**, followed by 216, 183, and 15 for Ni(OH)$_2$, PT/C, and bare FTO, respectively. A higher ECSA more catalytic sites which, in turn, depicts a higher catalytic performance. The ECSA (in cm^2) of **MOF 1** was much higher than that for materials reported, such as NiS$_2$–MoS$_2$ (1.45), NiS$_2$ (0.44),[26] Ni/Ni(OH)$_2$ (54), β Ni(OH)$_2$ (14),[15] Li$_4$Ni$_3$O$_{10}$ (8.98), Li$_2$NiO$_4$ (5.55), and Li$_3$Ni$_2$O$_7$ (6.33).[52] The mass activity was calculated by J m^{-1} (where J is the current density (10 mA cm^{-2}) at potential (1.24 V) and m is the mass loading (0.32 mg cm^{-2}) on an electrode surface.[53] The mass activity of **MOF 1** (31.25 A g^{-1}) was estimated to determine the intrinsic activity. The mass activity of **MOF 1** was 2.6- and 4.5-times greater than that of Ni-MIL-53-NH$_2$ (12 A g^{-1}) and Fe-MIL-53-NH$_2$ (6.8 A g^{-1}), respectively.[54] Thus, the outstanding activity of **MOF 1** for the UOR was credited to a high intrinsic activity and large ECSA. Recently, it has been reported that introduction of readily oxidizable metals in catalysts promotes oxidation reactions.[55] Thus, the ease of oxidation of Ni^{2+} to Ni^{3+} by application of potential during the UOR is correlated to its efficient activity.

Electrochemical impedance spectroscopy (EIS) was undertaken to obtain further insights about kinetics on the electrode/electrolyte interface during the UOR. Nyquist plots along with
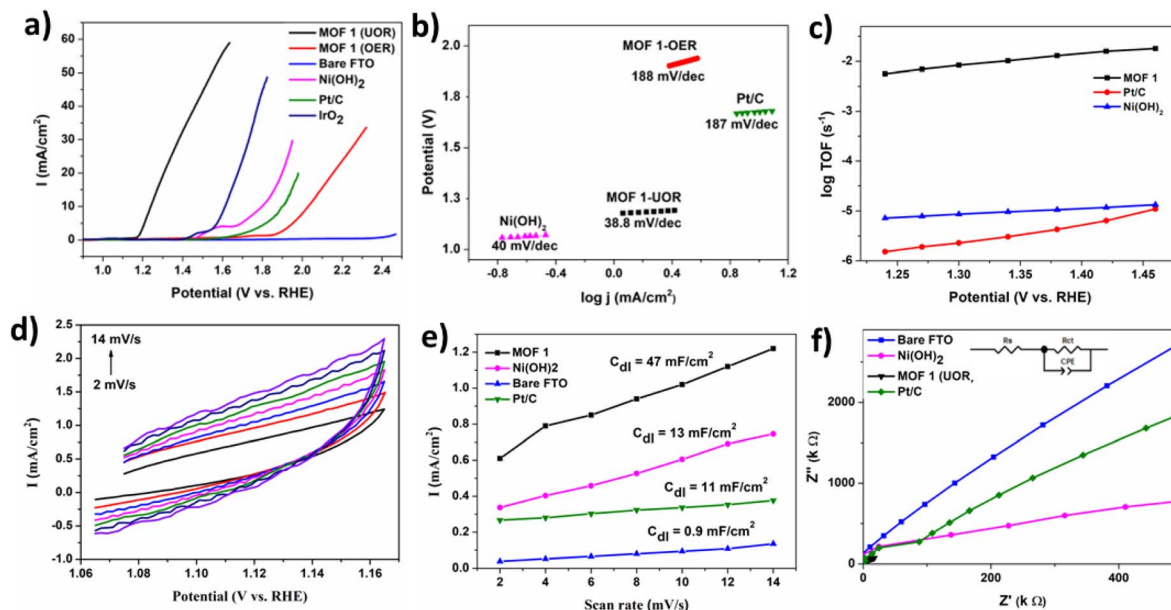
Fig. 2 (a) Linear sweep voltammetry for **MOF 1**, UOR, OER, and comparative materials *vs.* RHE. (b) Corresponding Tafel plots. (c) Dependence of the TOF in KOH (1 M) with urea (0.33 M). (d) Cyclic voltammetry in a non-faradaic region with an incremental sweep rate of 2 mV s^{-1}. (e) Current density (*I*) as a function of the sweep rate to determine C_{dl}. (f) Comparative Nyquist plots and equivalent circuits.

equivalent circuits are displayed in Fig. 2f in a frequency range of 100 kHz to 0.1 Hz. The smaller semi-circular diameter for **MOF 1** revealed the strikingly small resistance to charge transfer and, thus, high performance compared with that of Ni(OH)$_2$, Pt/C and bare FTO. The turnover frequency (TOF) was evaluated from the surface concentration of coated FTO to evaluate catalytic performance further. Assuming that all metal sites were electrocatalytically active, a potential of 1.24 V was required for a TOF of 5×10^{-3} s^{-1} at 10 mA cm^{-2} (Fig. 2c), which is greater than the TOF for Ni(OH)$_2$ (1.3×10^{-3} s^{-1}) and 2.9×10^{-4} s^{-1} for Pt/C. The TOF for **MOF 1** was also higher than that reported for Ni-MIL-53-NH$_2$ (1.2×10^{-3} s^{-1}) and Fe-MIL-53-NH$_2$ (6.5×10^{-4} s^{-1}).[54]

Another critical factor for the efficiency of a catalyst is its stability and durability for commercial applications. CPE was carried out for **MOF 1** at a potential of 1.41 V for 17 h ($J = 30$ mA cm^{-2}). **MOF 1** exhibited strong durability with retained UOR activity after 17 h continuously (Fig. 3a). The slight increment in current may be due to conversion of Ni(II) to Ni(III) during pre-oxidation to acquire high-valence, catalytically active Ni(III) species.[13] The electrochemical stability of **MOF 1** is compared to that of other Ni-based electrocatalysts from the literature. The stability of MOFs such as Ni-MOF-0.5,[42] 2D Ni-MOF,[43] Ni-MOF-100,[56] NiO@Ni-MOF,[48] NiMn$_{0.14}$-BDC MOF,[57] and 3% CeO$_2$/Ni-MOF has been documented.[58] LSV was undertaken after a long-term stability test. There was no noticeable change in the position of the curve for the initial scan and after the stability test. Fig. 3b shows the robustness of the catalyst. Taken together, these results suggest that **MOF 1** could be a potent electrocatalyst for the UOR.

Table 1 Comparative studies on reported UOR electrocatalysts with the present work

| Material	Electrolyte (1 M KOH)	Onset-potential (V)	Ref.
MOF 1	**+0.33 M urea**	**1.18**	**Present work**
NiFe-MIL-53-NH$_2$	+0.33 M urea	1.36	54
Ni-MOF@NiO/Ni	+0.33 M urea	1.40 (10 mA cm^{-2})	59
Aggregated Ni-MOF nanosheets	+0.5 M urea	1.38 (10 mA cm^{-2})	42
Ni$_3$N nanosheets	+0.33 M urea	1.33	60
Ni$_{0.9}$Fe$_{0.1}$O	+0.33 M urea	1.35	32
Ni(OH)$_2$	+0.33 M urea	1.36	15
Ni-Mo nanotubes	+0.1 M urea	1.36	33
Ni-MOF nanosheets	+0.1 M urea	1.33	50
Ni$_2$P/Fe$_2$P	+0.5 M urea	1.33	61
MnO$_2$/MnCo$_2$O$_4$/Ni	+0.5 M urea	1.33	33
Ni(OH)$_2$@NF	+0.33 M urea	1.33	62
Ni-B$_i$	+0.33 M urea	1.34	63
Ni-WO$_2$@C/NF	+0.33 M urea	1.30	64
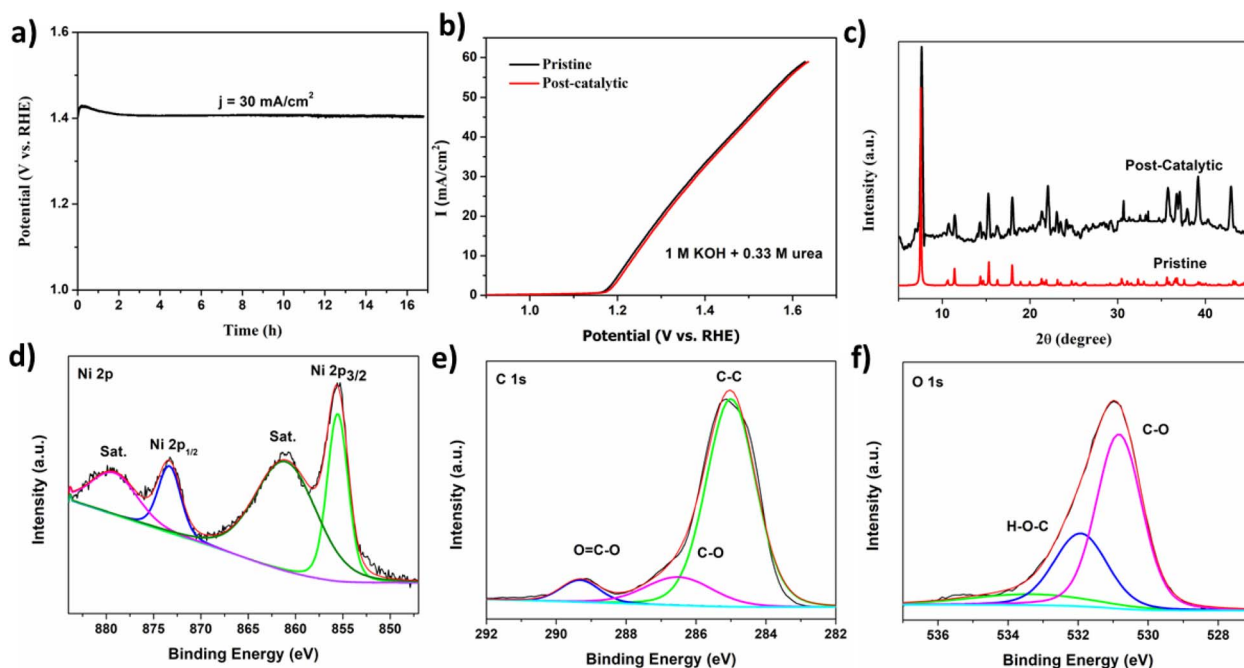
Fig. 3 (a) Controlled potential electrolysis at a potential of 1.41 V. (b) LSV curves of pristine and post-catalytic samples. Physiochemical structure of **MOF 1** after 17 h of continuous UOR electrolysis. (c) XRD spectrum of pristine and post-catalytic samples. (d) High-resolution spectra for Ni 2p (e) and C 1s (f) O 1s in post-catalytic samples.

The structural integrity of the catalyst was assessed before and after stability tests through PXRD, SEM, and X-ray photoelectron spectroscopy (XPS). A noticeable dissimilarity in the diffraction pattern for **MOF 1** before and after catalysis was not observed (Fig. 3c), which indicated the stability of the crystal structure after the UOR. The surface morphology of **MOF 1** remained intact after a 17 h stability test (Fig. S7†). To obtain information about the chemical composition and surface electronic state of **MOF 1**, XPS was employed in a post-catalytic sample. In the high-resolution Ni 2p spectrum, peaks at 855.6 and 873.2 eV were assigned to the core levels of Ni $2p_{3/2}$ and Ni $2p_{1/2}$, whereas shoulder peaks at 861.8 and 879 eV indicated the Ni^{2+} oxidation state (Fig. 3d).[65] The absence of Ni(0) and NiO peaks suggested that the catalyst was stable and was not converted to metallic nickel or its oxides. The XPS patterns for C 1s and O 1s are in accordance with the literature. The high-resolution C 1s spectrum showed distinctive peaks at 284.81 eV for C–C,[66] 286.5 eV for C–O, and 289.18 eV for O–C=O.[67] In the XPS pattern for O 1s, the deconvoluted peak at 530.81 eV corresponded to M–O, the peak at 532.1 eV was ascribed to C=O, and unavoidable adsorbed H_2O appeared at 534 eV.[68] The XPS survey is given in Fig. S8.†

Proposed mechanism

To understand the structure–activity relationship of **MOF 1** with abundantly exposed active sites we propose a mechanism involving fast transfer of electrons and low resistance to charge transfer. In an indirect or electrochemical–chemical (EC) mechanism, urea is oxidized to N_2, CO_2, and H_2O with catalyst regeneration:[69,70]

$$6Ni(OH)_2 + 6OH^- \rightarrow 6NiOOH + 6H_2O + 6e^-$$

$$6NiOOH + CO(NH_2)_2 + H_2O \rightarrow CO_2 + N_2 + 6Ni(OH)_2$$
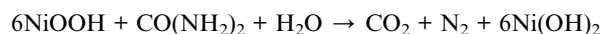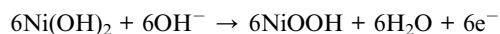
OH^- coordinated with Ni(II) in linear chains and dangling OH^- groups attached to Ni_4O_4 cubane makes $Ni\cdots OH^-$ prone to conversion to NiOOH under an applied potential during the UOR. Due to electrostatic interaction, the urea molecule is adsorbed on the active NiOOH surface *via* O–C and Ni–O coordination bonds.[71] As a result, urea is oxidized and NiOOH is reduced back to $Ni\cdots OH^-$ to complete the catalytic cycle, and reacts with OH^- to repeat the process.

Conclusions

We identified **MOF 1** as a unique electrocatalyst that exhibits excellent activity, strong durability, and stability along with favorable kinetics towards the UOR. The low onset potential of 1.18 V and Tafel slope of 38.8 mV dec^{-1} was due to an intrinsic high TOF of 0.005 s^{-1}. A lowest overpotential of 1.24 V to attain a catalytic current density of 10 mA cm^{-2} makes **MOF 1** a highly efficient electrocatalyst for the UOR. No considerable change in comparative PXRD patterns of a pristine sample and post-catalytic sample signified the structural stability of MOF. **MOF 1** could be a competent candidate for urea-associated applications such as hydrogen production, treatment of urea in wastewater, and urea-based fuel cells. Most importantly, our work provides insights for designing heterogenous catalysts at the molecular level. Thus, by incorporating suitable linkers, the

electronic environment around metals could be altered to make it conducive to the design of exceptional catalysts having high oxidation states for various oxidation reactions.

Author contributions

All authors contributed equally to this work.

Conflicts of interest

There are no conflicts to declare.

Acknowledgements

Notes and references

1 M. Dresselhaus and I. Thomas, *Nature*, 2001, **414**, 332.
2 Y. Xing, B. Fang, A. Bonakdarpour, S. Zhang and D. P. Wilkinson, *Int. J. Hydrogen Energy*, 2014, **39**, 7859.
3 P. Hao, W. Zhu, L. Li, J. Tian, J. Xie, F. Lei, G. Cui, G. Y. Zhang and B. Tang, *Electrochim. Acta*, 2020, **338**, 135883.
4 M. Carmo, D. L Fritz, J. Mergel and D. Stolten, *Int. J. Hydrogen Energy*, 2013, **38**, 4901.
5 X. Sun and R. Ding, *Catal. Sci. Technol.*, 2020, **10**, 1567.
6 J. Jiang, L. Chang, W. Zhao, Q. Tian and Q. Xu, *ChemComm*, 2019, **55**, 10174.
7 C. Tang, R. Zhang, W. Lu, Z. Wang, D. Liu, S. Hao, G. Du, A. M. Asiri and X. Sun, *Angew. Chem., Int. Ed.*, 2017, **56**, 842.
8 J. Xie, L. Gao, S. Cao, W. Liu, F. Lei, P. Hao, X. Xia and B. Tang, *J. Mater. Chem. A*, 2019, **7**, 13577.
9 X. Yang, L. Kang, Z. Wei, S. Lou, F. Lei, P. Hao, J. Xie and B. Tang, *Chem. Eng. J.*, 2021, **422**, 130139.
10 J. Zhang, J. H. Wang, Y. Tian, Y. Yan, Q. Xue, T. He, H. Liu, C. Wang, Y. Chen and B. Y. Xia, *Angew. Chem., Int. Ed.*, 2018, **57**, 7649.
11 M. N. Kopylovich, A. P. Ribeiro, E. C. Alegria, N. M. Martins, L. M. Martins and A. J. Pombeiro, *Adv. Organomet. Chem.*, 2015, **63**, 91.
12 H. G. Cha and K. S. Choi, *Nat. Chem.*, 2015, **7**, 328.
13 J. Xie, W. Liu, F. Lei, X. Zhang, H. Qu, L. Gao, P. Hao, B. Tang and Y. Xie, *Chem.–Eur. J.*, 2018, **24**, 18408.
14 W. Liu, J. Xie, Y. Guo, S. Lou, L. Gao and B. Tang, *J. Mater. Chem. A*, 2019, **7**, 24437.
15 R. K. Singh and A. Schechter, *Electrochim. Acta*, 2018, **278**, 405.
16 J. Xie, W. Liu, X. Zhang, Y. Guo, L. Gao, F. Lei, B. Tang and Y. Xie, *ACS Mater. Lett.*, 2019, **1**, 103.
17 X. Zhu, X. Dou, J. Dai, X. An, Y. Guo, L. Zhang, S. Tao, J. Zhao, W. Chu and X. C. Zeng, *Angew. Chem., Int. Ed.*, 2016, **55**, 12465.
18 F. Wu, G. Ou, Y. Wang, H. Zhong, L. Zhang, H. Li and Y. Shi, *Chem.–Asian J.*, 2019, **14**, 2796.
19 J. Xie, H. Qu, F. Lei, X. Peng, W. Liu, L. Gao, P. Hao, G. Cui and B. Tang, *J. Mater. Chem. A*, 2018, **6**, 16121.
20 Z. Wei, W. Sun, S. Liu, J. Qi, L. Kang, J. Li, S. Lou, J. Xie, B. Tang and Y. Xie, *Particuology*, 2021, **57**, 104.
21 W. Simka, J. Piotrowski, A. Robak and G. Nawrat, *J. Appl. Electrochem.*, 2009, **39**, 1137.
22 J. Wright, A. Michaels and A. Appleby, *AIChE J.*, 1986, **32**, 1450.
23 W. Simka, J. Piotrowski and G. Nawrat, *Electrochim. Acta*, 2007, **52**, 5696.
24 A. Bolzan and T. Iwasita, *Electrochim. Acta*, 1988, **33**, 109.
25 B. K. Boggs, R. L. King and G. G. Botte, *ChemComm*, 2009, **32**, 4859.
26 S. Wang, L. Zhao, J. Li, X. Tian, X. Wu and L. Feng, *J. Energy Chem.*, 2022, **66**, 483.
27 S. Wang, J. Zhu, X. Wu and L. Feng, *Chin. Chem. Lett.*, 2022, **33**, 1105.
28 P. Hao, H. Wen, Q. Wang, L. Li, Z. Zhao, R. Xu, J. Xie, G. Cui and B. Tang, *J. Mater. Chem. A*, 2021, **9**, 8576.
29 D. Suárez, N. Díaz and K. M. Merz, *J. Am. Chem. Soc.*, 2003, **125**, 15324.
30 J. Li, S. Wang, J. Chang and L. Feng, *Adv. Powder Mater.*, 2022, **3**, 100030.
31 Q. Liu, L. Xie, F. Qu, Z. Liu, G. Du, A. M. Asiri and X. Sun, *Inorg. Chem. Front.*, 2017, **4**, 1120.
32 F. Wu, G. Ou, J. Yang, H. Li, Y. Gao, F. Chen, Y. Wang and Y. Shi, *ChemComm*, 2019, **55**, 6555.
33 J. Y. Zhang, T. He, M. Wang, R. Qi, Y. Yan, Z. Dong, H. Liu, H. Wang and B. Y. Xia, *Nano Energy*, 2019, **60**, 894.
34 S. Zhao, Y. Wang, J. Dong, C. T. He, H. Yin, P. An, K. Zhao, X. Zhang, C. Gao and L. Zhang, *Nat. Energy*, 2016, **1**, 1.
35 J. H. Kim, B. Fang, M. Y. Song and J. S. Yu, *Chem. Mater.*, 2012, **24**, 2256.
36 B. Fang, J. H. Kim, M. S. Kim and J. S. Yu, *Acc. Chem. Res.*, 2013, **46**, 1397.
37 B. Fang, L. Daniel, A. Bonakdarpour, R. Govindarajan, J. Sharman and D. P. Wilkinson, *Small*, 2021, **17**, 2102288.
38 L. Lu, S. Zou and B. Fang, *ACS Catal.*, 2021, **11**, 6020.
39 B. Fang, J. H. Kim and J. S. Yu, *Electrochem. Commun.*, 2008, **10**, 659.
40 Z. Gao, Y. Wang, L. Xu, Q. Tao, X. Wang, Z. Zhou, Y. Luo, J. Yu and Y. Huang, *Chem. Eng. J.*, 2022, **433**, 133515.
41 Q. Li, S. Zheng, M. Du and H. Pang, *Chem. Eng. J.*, 2021, **417**, 129201.
42 S. Zheng, Y. Zheng, H. Xue and H. Pang, *Chem. Eng. J.*, 2020, **395**, 125166.
43 D. Zhu, C. Guo, J. Liu, L. Wang, Y. Du and S. Z. Qiao, *ChemComm*, 2017, **53**, 10906.
44 L. Wang, L. Ren, X. Wang, X. Feng, J. Zhou and B. Wang, *ACS Appl. Mater. Interfaces*, 2018, **10**, 4750.
45 S. Rezaee and S. Shahrokhian, *Nanoscale*, 2020, **12**, 16123.
46 M. A. Nadeem, M. C. C. Ng, J. van Leusen, P. Kögerler and J. A. Stride, *Chem.–Eur. J.*, 2020, **26**, 7589.

47 M. Radhika, B. Gopalakrishna, K. Chaitra, L. K. G. Bhatta, K. Venkatesh, M. S. Kamath and N. Kathyayini, *Mater. Res. Express*, 2020, **7**, 054003.

48 S. Xiong, S. Jiang, J. Wang, H. Lin, M. Lin, S. Weng, S. Liu, Y. Jiao, Y. Xu and J. A. Chen, *Electrochim. Acta*, 2020, **340**, 135956.

49 R. P. Forslund, J. T. Mefford, W. G. Hardin, C. T. Alexander, K. P. Johnston and K. J. Stevenson, *ACS Catal.*, 2016, **6**, 5044.

50 D. Zhu, C. Guo, J. Liu, L. Wang, Y. Du and S.-Z. Qiao, *ChemComm*, 2017, **53**, 10906.

51 S. Hu, C. Feng, S. Wang, J. Liu, H. Wu, L. Zhang and J. Zhang, *ACS Appl. Mater. Interfaces*, 2019, **11**, 13168.

52 Y. Tao, L. Chen, Z. Ma, C. Zhang, Y. Zhang, D. Zhang, D. Pan, J. Wu and G. Li, *Chem. Eng. J.*, 2022, **446**, 137240.

53 J. Huang, J. Chen, T. Yao, J. He, S. Jiang, Z. Sun, Q. Liu, W. Cheng, F. Hu and Y. Jiang, *Angew. Chem., Int. Ed.*, 2015, **127**, 8846.

54 Z. Gao, Y. Wang, L. Xu, Q. Tao, X. Wang, Z. Zhou, Y. Luo, J. Yu and Y. Huang, *Chem. Eng. J.*, 2022, **433**, 133515.

55 C. Guo, Y. Zheng, J. Ran, F. Xie, M. Jaroniec and S. Z. Qiao, *Angew. Chem., Int. Ed.*, 2017, **56**, 8539.

56 M. Yuan, R. Wang, Z. Sun, L. Lin, H. Yang, H. Li, C. Nan, G. Sun and S. Ma, *Inorg. Chem.*, 2019, **58**, 11449.

57 X. Xu, Q. Deng, H. C. Chen, M. Humayun, D. Duan, X. Zhang, H. Sun, X. Ao and X. Xue, *Research*, 2022, **2022**, 9837109.

58 X. Wu, L. Li, J. Pan, X. Wang, H. Zhang, S. Song and H. Zhang, *Mater. Lab.*, 2022, **1**, 220009.

59 Q. Li, S. Zheng, M. Du and H. Pang, *Chem. Eng. J.*, 2021, **417**, 129201.

60 Q. Liu, L. Xie, F. Qu, Z. Liu, G. Du, A. M. Asiri and X. Sun, *Inorg. Chem.*, 2017, **4**, 1120.

61 H. Xu, K. Ye, K. Zhu, Y. Gao, J. Yin, J. Yan, G. Wang and D. Cao, *ACS Sustainable Chem. Eng.*, 2020, **8**, 16037.

62 L. Xia, Y. Liao, Y. Qing, H. Xu, Z. Gao, W. Li and Y. Wu, *ACS Appl. Energy Mater.*, 2020, **3**, 2996.

63 J. Ge, Y. Lai, M. Guan, Y. Xiao, J. Kuang and C. Yang, *Environ. Sci.: Nano*, 2021, **8**, 1326.

64 F. Shen, W. Jiang, G. Qian, W. Chen, H. Zhang, L. Luo and S. Yin, *J. Power Sources*, 2020, **458**, 228014.

65 L. Qian, Z. Lu, T. Xu, X. Wu, Y. Tian, Y. Li, Z. Huo, X. Sun and X. Duan, *Adv. Energy Mater.*, 2015, **5**, 1500245.

66 A. Thomas, A. Fischer, F. Goettmann, M. Antonietti and J. O. Müller, *J. Mater. Chem. A*, 2008, **18**, 4893.

67 H. Cao, X. Wu, G. Yin and J. H. Warner, *Inorg. Chem.*, 2012, **51**, 2954.

68 S. Dutta, A. Indra, Y. Feng, H. Han and T. Song, *Appl. Catal., B*, 2019, **241**, 521.

69 V. Vedharathinam and G. Botte, *Electrochim. Acta*, 2012, **81**, 292.

70 W. Sun, J. Li, W. Gao, L. Kang, F. Lei and J. Xie, *ChemComm*, 2022, **58**, 2430.

71 D. A. Daramola, D. Singh and G. G. Botte, *J. Phys. Chem. A*, 2010, **114**, 11513.